INTERNATIONAL JOURNAL FOR NUMERICAL METHODS IN FLUIDS, VOL. 14, 539–556 (1992)

THE NUMERICAL SOLUTION OF THE THIN FILM FLOW SURROUNDING A HORIZONTAL CYLINDER RESULTING FROM A VERTICAL CYLINDRICAL JET

ROLAND HUNT

Department of Mathematics, University of Strathclyde, George Street, Glasgow, G1 1XH, U.K.

SUMMARY

The numerical solution of the thin film flow surrounding a horizontal cylinder resulting from a single vertical cylindrical jet is obtained. This is effected by transforming the domain of the flow, which contains a free surface, onto a rectangular parallelepiped and using a marching strategy to solve the ensuing parabolic equations. The flow terminates at a finite distance along the cylinder, its position depending on the velocity and mass flux of the jet. A comparison with the usual two-dimensional model in which the jet is replaced by a vertical sheet shows that such a representation is valid provided the overall width of the flow is not too large. In particular, the differences in heat transfer characteristics amount to a few per cent, thus validating the use of the two-dimensional model when applied to heat exchanger tubes. A comparison with the more usual multicolumn case is also considered.

KEY WORDS Thin film flows Free boundary problems Parabolic differential equations

1. INTRODUCTION

Heat exchanger pipes in steam condensers are surrounded by a thin film of running water which arises from the condensation of steam onto cool pipes. Typically, a condenser will consist of an array of horizontal tubes with water draining from the one above to the one below. This drainage is usually in the form of equally spaced columns of liquid issuing from the midpoints of the columns of liquid associated with the tube one step higher (Figure 1(a)). This thin film of water significantly affects the heat transfer characteristics of the tubes and has been extensively studied both theoretically and experimentally.[1–5] In the theoretical treatment the columns of liquid are replaced by a vertical sheet of liquid which renders the governing equations independent of the direction along the tubes (Figure 1(b)). The problem is now two-dimensional and amenable to solution, whereas the original problem is three-dimensional and fairly untractable. The question that now arises concerns the accuracy of these results when applied to the original problem.

In this paper we seek to solve the thin film flow of a single vertical cylindrical column of liquid impinging onto the top generator of a horizontal cylinder (Figure 2). The study of a single column rather than an array of columns is chosen since the governing thin film equations are parabolic in nature and can be solved using a marching computer code. However, to solve the flow of an array of columns would necessitate that information should be capable of being passed from one column to another. In other words governing equations would need to be elliptic and hence we would need to use the full Navier–Stokes equations, which makes the problem an order of magnitude more difficult. The study of the single column is, however, a significant step forward,

0271–2091/92/050539–18$09.00

Received March 1991
Revised June 1991

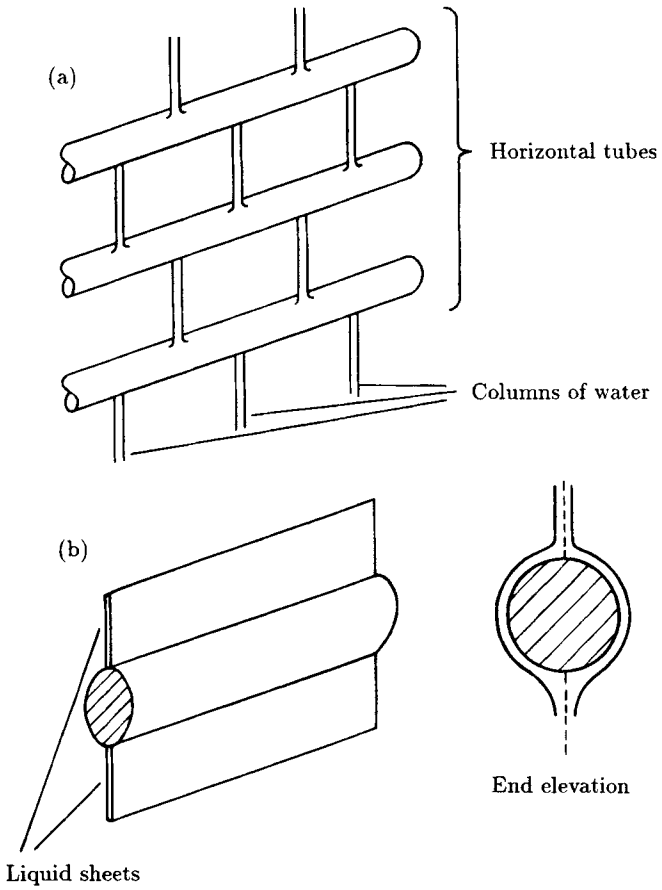

Figure 1. (a) Typical arrangement of horizontal tubes in a heat exchanger showing the columns of liquid falling in an alternate pattern. (b) The usual two-dimensional model used in theoretical calculations

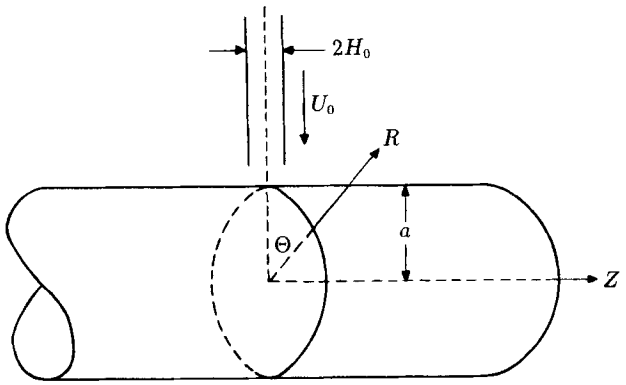

Figure 2. The three-dimensional model with a single column of liquid showing the co-ordinate system

being three-dimensional, and will enable us to successfully assess the results of the two-dimensional model.

The method of solution is an extension of that used for the two-dimensional flow about a cylinder described in an earlier paper[1] (referred to as Paper I). The governing equations are first formulated in terms of two streamfunctions (Section 2). The outer boundary of the thin film is a free surface and in order to obtain accurate numerical results, the domain of the fluid is transformed onto a rectangular parallelepiped.[6] The transformation used (see Section 3) not only gives a fixed domain but also removes the singularity at the origin since the flow is initially Blasius-like. Section 4 shows how these equations can be integrated numerically, which necessitates subtracting out the flow at the origin. The results, comparison with the two-dimensional model and our main conclusions are presented in Section 5.

2. GOVERNING EQUATIONS

A cylindrical jet of fluid having raduis H_0 and velocity U_0 impinges vertically on the top generator of a horizontal cylinder having radius a, upon which we impose cylindrical polar co-ordinates (R, Θ, Z) (Figure 2). In the large-Reynolds-number case the flow immediately subsequent to the jet forms a thin film of liquid. Since the film is thin, we can neglect the perpendicular velocity V_R compared to the surface velocities V_Θ and V_Z; further, we can neglect Θ- and Z-derivatives compared to R-derivatives. The Navier–Stokes and heat conduction equations in cylindrical polars co-ordinates then give

$$\begin{aligned}
&\frac{\partial V_R}{\partial R}+\frac{1}{a}\frac{\partial V_\Theta}{\partial \Theta}+\frac{\partial V_Z}{\partial Z}=0,\\
&V_R\frac{\partial V_\Theta}{\partial R}+\frac{V_\Theta}{a}\frac{\partial V_\Theta}{\partial \Theta}+V_Z\frac{\partial V_\Theta}{\partial Z}=g\sin\Theta+\nu\frac{\partial^2 V_R}{\partial^2 R},\\
&V_R\frac{\partial V_Z}{\partial R}+\frac{V_\Theta}{a}\frac{\partial V_Z}{\partial \Theta}+V_Z\frac{\partial V_Z}{\partial Z}=\nu\frac{\partial^2 V_Z}{\partial^2 R},\\
&V_R\frac{\partial T}{\partial R}+\frac{V_\Theta}{a}\frac{\partial T}{\partial \Theta}+V_Z\frac{\partial T}{\partial Z}=\kappa\frac{\partial^2 T}{\partial^2 R},
\end{aligned} \tag{1}$$

where T, g, ν and κ are the temperature, the acceleration due to gravity, the kinematic viscosity and the thermal diffusivity respectively. This derivation is similar to that involved in obtaining the boundary layer equations and similarly shows that the pressure is independent of R. This implies that if the pressure on the film surface is assumed constant (as in a steam condenser) then it is constant throughout the film and hence does not appear in the equations.

Letting $H(\Theta, Z)$ be the thickness of the film, the position of the outer boundary can be denoted by $\Phi=0$, where $\Phi\equiv a+H(\Theta, Z)-R$. Demanding that the velocity vector $\mathbf{V}\equiv(V_R, V_\Theta, V_Z)$ lies in the surface of the film requires that $\nabla\Phi\cdot\mathbf{V}=0$, which gives the boundary condition

$$\frac{V_\Theta}{a}\frac{\partial H}{\partial \Theta}+V_Z\frac{\partial H}{\partial Z}-V_R=0 \quad \text{on } R=a+H(\Theta, Z). \tag{2}$$

The other boundary conditions are the no-slip condition $V_R=V_\Theta=V_Z=0$ on $R=a$, zero shear $\partial V_\Theta/\partial R=\partial V_Z/\partial R=0$ on the surface $R=a+H(\Theta, Z)$, $T=T_w$ on $R=a$ and $T=T_s$ on $R=a+H(\Theta, Z)$, where T_w and T_s are the temperatures on the cylinder wall and free surface respectively.

Near the jet the cylinder is approximately horizontal and the flow is radially symmetric. The flow here is essentially inviscid since, the jet Reynolds number U_0H_0/ν being much less than the Reynolds number U_0a/ν of the film, the viscous boundary layer has not yet developed. Hence Bernouilli's equation can be used to show that the radial velocity U initially has a uniform profile of magnitude U_0. If $\bar{R}$ is the radial distance from the centre of the jet then conservation of mass requires that $\pi H_0^2 U_0 = 2\pi \bar{R} H U$. Hence initially the conditions are

$$U \to U_0 \quad \text{and} \quad H \to \tfrac{1}{2} H_0^2/\bar{R} \quad \text{as } \bar{R} \to 0. \tag{3}$$

Equations (1) can be non-dimensionalized using

$$\Theta = y, \qquad Z = ax, \qquad R = a + \frac{a}{Re^{1/2}} z, \qquad H = \frac{a}{Re^{1/2}} h,$$

$$V_Z = U_0 u, \qquad V_\Theta = U_0 v, \qquad V_R = \frac{U_0}{Re^{1/2}} w, \qquad \theta = \frac{T - T_s}{T_w - T_s}, \tag{4}$$

where $Re = U_0 a/\nu$ is the Reynolds number, to give

$$\begin{aligned}
&\frac{\partial u}{\partial x} + \frac{\partial v}{\partial y} + \frac{\partial w}{\partial z} = 0, \\
&u\frac{\partial u}{\partial x} + v\frac{\partial u}{\partial y} + w\frac{\partial u}{\partial z} = \frac{\partial^2 u}{\partial^2 z}, \\
&u\frac{\partial v}{\partial x} + v\frac{\partial v}{\partial y} + w\frac{\partial v}{\partial z} = \frac{1}{F}\sin y + \frac{\partial^2 v}{\partial^2 z}, \\
&u\frac{\partial \theta}{\partial x} + v\frac{\partial \theta}{\partial y} + w\frac{\partial \theta}{\partial z} = \frac{1}{\sigma}\frac{\partial^2 \theta}{\partial^2 z},
\end{aligned} \tag{5}$$

where $F = U_0^2/ga$ is the Froude number and $\sigma = \nu/\kappa$ is the Prandtl number. The boundary conditions then are

$$\begin{aligned}
&u = v = w = 0 \quad \text{and} \quad \theta = 1 \quad \text{on } z = 0, \\
&\frac{\partial u}{\partial z} = \frac{\partial v}{\partial z} = 0, \quad u\frac{\partial h}{\partial x} + v\frac{\partial h}{\partial y} - w = 0 \quad \text{and} \quad \theta = 0 \quad \text{on } z = h(x, y), \\
&u \to \frac{x}{r}, \quad v \to \frac{y}{r} \quad \text{and} \quad h \to \frac{\gamma}{r} \quad \text{as } r \to 0,
\end{aligned} \tag{6}$$

where $r = \sqrt{(x^2 + y^2)}$ and $\gamma = \tfrac{1}{2} Re^{1/2} (H_0/a)^2$.

To tie in with previous work, we introduce streamfunctions ϕ and ψ defined by

$$u = \frac{\partial \psi}{\partial z}, \qquad v = \frac{\partial \phi}{\partial z}, \qquad w = -\frac{\partial \psi}{\partial x} - \frac{\partial \phi}{\partial y}, \tag{7}$$

which implies that the first of (5) is satisfied identically. The other three equations of (5) give

$$\begin{aligned}
&\psi_{zzz} = (\psi_z \psi_{xz} - \psi_x \psi_{zz}) + (\phi_z \psi_{yz} - \phi_y \psi_{zz}), \\
&\phi_{zzz} + \frac{1}{F}\sin y = (\psi_z \phi_{xz} - \psi_x \phi_{zz}) + (\phi_z \phi_{yz} - \phi_y \phi_{zz}), \\
&\frac{1}{\sigma}\theta_{zz} = (\psi_z \theta_x - \psi_x \theta_z) + (\phi_z \theta_y - \phi_y \theta_z),
\end{aligned} \tag{8}$$

subject to boundary conditions

$$\begin{gathered}\psi_z=\phi_z=0, \quad \psi=\phi=0 \quad \text{and} \quad \theta=1 \quad \text{on } z=0,\\ \psi_{zz}=\phi_{zz}=0, \quad \psi_z h_x+\phi_z h_y+\psi_x+\phi_y=0 \quad \text{and} \quad \theta=0 \quad \text{on } z=h(x,y),\\ \psi_z\to\frac{x}{r}, \quad \phi_z\to\frac{y}{r} \quad \text{and} \quad h\to\frac{\gamma}{r} \quad \text{as } r\to 0,\end{gathered} \tag{9}$$

where conditions $\psi=\phi=0$ on $z=0$ define ψ and ϕ uniquely.

The governing equations for the two-dimensional model in which the cylindrical jet is replaced by a sheet of liquid can be found from equations (8) by putting $\psi=0$ and $\partial/\partial x=0$ (see Paper I) to give

$$\begin{gathered}\phi_{zzz}+\frac{1}{F}\sin y=\phi_z\phi_{yz}-\phi_y\phi_{zz},\\ \frac{1}{\sigma}\theta_{zz}=\phi_z\theta_y-\phi_y\theta_z,\end{gathered} \tag{10}$$

subject to boundary conditions

$$\begin{gathered}\phi_z=0, \quad \phi=0 \quad \text{and} \quad \theta=1 \quad \text{on } z=0,\\ \phi_{zz}=0, \quad \phi=\gamma_2 \quad \text{and} \quad \theta=0 \quad \text{on} \quad z=h(y),\\ \phi\to z \quad \text{and} \quad h\to\gamma_2 \quad \text{as } r\to 0,\end{gathered} \tag{11}$$

where $\gamma_2=Re^{1/2}H_2/a$ and H_2 is the semithickness of the impinging sheet.

3. TRANSFORMATION OF THE EQUATIONS

As in Paper I, we solve the free boundary problem (8), (9) by transforming the unknown domain of fluid onto a rectangular parallelepiped. More explicitly, we replace the independent variables (x, y, z) by (x, y, η) using the transformation $z=z(x, y, \eta)$ chosen such that the interval $0\leqslant z\leqslant h(x, y)$ is mapped onto the interval $0\leqslant\eta\leqslant 1$. Secondly, this transformation is chosen such that the inconsistency in the boundary conditions at the source is removed. From (9) we observe that $\psi_z=\phi_z=0$ on $z=0$, which is contrary to the condition that $\psi_z\to x/r$ and $\phi_z\to y/r$ as $r\to 0$. This inconsistency is removed in boundary layer theory using the Blasius transformation. However, here we need to use a more general transformation if we are simultaneously to maintain the fluid within a rectangular parallelepiped. We proceed as follows.

First we write equations (8) as a first-order system since they will be solved numerically in this form and it makes the algebra much more tractable. In vector form these become

$$\begin{gathered}D\mathbf{w}_z+\mathbf{f}=(\bar{\mathbf{u}}\cdot\bar{\nabla})\mathbf{u}-\mathbf{w}\bar{\nabla}\cdot\bar{\mathbf{\Psi}},\\ \bar{\mathbf{\Psi}}_z=\bar{\mathbf{u}}, \qquad \mathbf{u}_z=\mathbf{w},\end{gathered} \tag{12}$$

where unbarred quantities are three-dimensional,

$$\mathbf{u}=\begin{pmatrix}\psi_z\\ \phi_z\\ \theta\end{pmatrix}, \qquad \mathbf{w}=\begin{pmatrix}\psi_{zz}\\ \phi_{zz}\\ \theta_z\end{pmatrix}, \qquad \mathbf{f}=\frac{1}{F}\begin{pmatrix}0\\ \sin y\\ 0\end{pmatrix}, \qquad D=\begin{pmatrix}1 & 0 & 0\\ 0 & 1 & 0\\ 0 & 0 & 1/\sigma\end{pmatrix},$$

and barred quantities are two-dimensional,

$$\bar{\boldsymbol{\Psi}}=\begin{pmatrix}\psi\\ \phi\end{pmatrix}, \qquad \bar{\mathbf{u}}=\begin{pmatrix}\psi_z\\ \phi_z\end{pmatrix}, \qquad \bar{\nabla}=\begin{pmatrix}\partial/\partial x\\ \partial/\partial y\end{pmatrix}. \tag{13}$$

This mixture of dimensions is necessary if both the Navier–Stokes and the heat conduction equations are to be written as a single equation.

We then make the general transformation $z=z(x, y, \eta)$ of the independent variables and transform the dependent variables using

$$\bar{\boldsymbol{\Psi}}=g\tilde{\bar{\boldsymbol{\Psi}}}, \qquad \mathbf{w}=\tilde{\mathbf{w}}/g, \tag{14}$$

where g depends on x, y and η and will be chosen to ensure that tilded variables are finite and $O(1)$ over the whole domain. Equations (12) then become

$$\begin{gathered}D\left(\mathbf{w}_\eta-\frac{g_\eta}{g}\mathbf{w}\right)+s(\bar{\boldsymbol{\Psi}}\cdot\bar{\nabla}g)\mathbf{w}+sg\mathbf{f}=sg[(\bar{\mathbf{u}}\cdot\bar{\nabla})\mathbf{u}-\mathbf{w}\bar{\nabla}\cdot\bar{\boldsymbol{\Psi}}],\\ \bar{\boldsymbol{\Psi}}_\eta=\frac{s}{g}\bar{\mathbf{u}}-\frac{g_\eta}{g}\bar{\boldsymbol{\Psi}}, \qquad \mathbf{u}_\eta=\frac{s}{g}\mathbf{w},\end{gathered} \tag{15}$$

where the tildes have been dropped for clarity and $s=\partial z/\partial\eta$.

Immediately subsequent to the jet we have an outward axisymmetric flow whose variables can be written as an expansion in powers of $r^{3/2}$ (as is typical of the analysis of a growing boundary layer in axisymmetric geometry). Similar to the axisymmetric flows in Paper I, this leads to a choice of transformation and g given by

$$z=\frac{r^{1/2}\eta\bar{h}}{r^{3/2}+1-\eta}, \qquad g=\frac{r^{1/2}}{r^{3/2}+1-\eta}, \tag{16}$$

where $\bar{h}=rh$ is the scaled film thickness. Equations (16) map the interval $0\leqslant z\leqslant h(x, y)$ onto $0\leqslant\eta\leqslant 1$ and ensure that all dependent variables including $\bar{h}$ are $O(1)$ over the whole domain. The only drawback is that whilst (16) successfully deal with the inconsistency in the boundary conditions, it has created a co-ordinate singularity at $r=0$, $\eta=1$. Fortunately, however, the flow here is extremely uniform and does not unduly affect the accuracy of the results. As explained in Paper I, there does not seem to be a transformation which will have all the required properties and avoid this singularity. Setting $\xi=r^{3/2}$, th elements in equation (15) are

$$\begin{gathered}\frac{g_\eta}{g}=\frac{1}{\xi+1-\eta}, \qquad s\bar{\nabla}g=\begin{pmatrix}x/r\\ y/r\end{pmatrix}sg_r, \quad \text{where } sg_r=\frac{(1-\eta-2\xi)(\xi+1)\bar{h}}{2(\xi+1-\eta)^4},\\ sg=\frac{r(\xi+1)\bar{h}}{(\xi+1-\eta)^3}, \qquad \frac{s}{g}=\frac{(\xi+1)\bar{h}}{\xi+1-\eta}.\end{gathered} \tag{17}$$

Boundary conditions (9) become

$$\begin{gathered}\bar{\boldsymbol{\Psi}}=0 \quad \text{and} \quad \mathbf{u}=(0, 0, 1)^{\mathrm{T}} \quad \text{on } \eta=0,\\ \bar{\boldsymbol{\Psi}}_{zz}=0, \quad \psi_x+\phi_y=0 \quad \text{and} \quad \theta=0 \quad \text{on } \eta=1.\end{gathered} \tag{18}$$

Initial and boundary equations

The problem is symmetrical about the planes $x=0$ and $y=0$ and hence it is sufficient to solve the problem in the quarter-plane $x\geqslant 0$, $y\geqslant 0$. Since equations (15) are parabolic in both the x- and

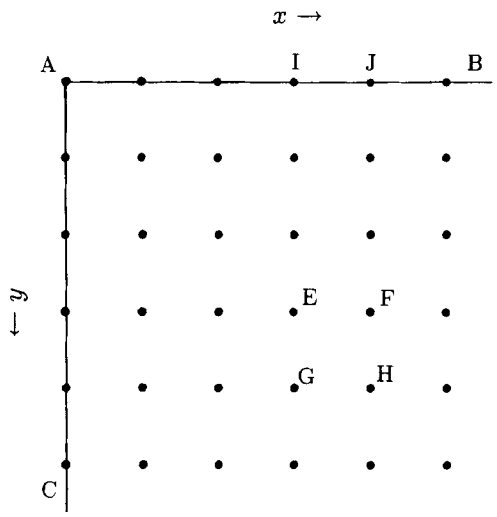

Figure 3. The computational grid in the xy-plane

y-directions, it is possible to solve the problem by marching in both of these directions. Suppose a uniform mesh is placed on the quarter-plane (Figure 3); then it is possible to obtain a solution of (15) at location H along $0 \leqslant \eta \leqslant 1$ provided the solution at points E, F and G is known. Hence it is possible to obtain a solution in the open quarter-plane $x>0$, $y>0$ provided a solution is available along lines AB and AC.

The governing equations along AB and AC are more easily derived by considering the equations in polar form; that is, independent variables x and y are replaced by r and τ using substitution $x=r\cos\tau$, $y=r\sin\tau$. The first two equations of (8) become

$$\hat{\psi}_{zzz}+\frac{1}{r}\hat{\psi}\hat{\psi}_{zz}+\frac{1}{r}\hat{\phi}_z^2+\frac{1}{F}\sin(r\sin\tau)\sin\tau=(\hat{\psi}_z\hat{\psi}_{rz}-\hat{\psi}_r\hat{\psi}_{zz})+(\hat{\phi}_z\hat{\psi}_{rz}-\hat{\phi}_r\hat{\psi}_{zz}), \tag{19a}$$

$$\hat{\phi}_{zzz}+\frac{1}{r}\hat{\psi}\hat{\phi}_{zz}-\frac{1}{r}\hat{\psi}_z\hat{\phi}_z+\frac{1}{F}\sin(r\sin\tau)\cos\tau=(\hat{\psi}_z\hat{\phi}_{rz}-\hat{\psi}_r\hat{\phi}_{zz})+(\hat{\phi}_z\hat{\phi}_{rz}-\hat{\phi}_r\hat{\phi}_{zz}), \tag{19b}$$

where $\hat{\psi}$ and $\hat{\phi}$ are the radial and meridional streamfunctions given by $\hat{\psi}=\psi\cos\tau+\phi\sin\tau$ and $\hat{\phi}=-\psi\sin\tau+\phi\cos\tau$. The lines AB and AC are lines of symmetry about which $\hat{\psi}$ is an even function and $\hat{\phi}$ is odd, making every term in equation (19b) zero. However, a second non-zero equation is needed to complete the system and this is found by differentiating (19b) with respect to τ. Introducing $q=(1/r)\partial\hat{\phi}/\partial\tau$, equations (19) along AB and AC become

$$\hat{\psi}_{zzz}+\frac{1}{r}\hat{\psi}\hat{\psi}_{zz}+\hat{\psi}_z q+\frac{1}{F}f_1=(\hat{\psi}_z\hat{\psi}_{rz}-\hat{\psi}_r\hat{\psi}_{zz}),$$

$$q_{zzz}+\frac{1}{r}\hat{\psi}q_{zz}+q_z q-q^2-\frac{2}{r}\hat{\psi}_z q_z+\frac{1}{F}f_2=(\hat{\psi}_z\hat{q}_{rz}-\hat{\psi}_r\hat{q}_{zz}), \tag{20}$$

where $f_1=0$, $f_2=1$ along $\tau=0$ (AB) and $f_1=(\sin y)/y, f_2=\sin y$ along $\tau=\pi/2$ (AC). Using the transformations (14) and (16), the full set of equations along AB and AC is

$$D\left(\hat{\mathbf{w}}_\eta-\frac{g_\eta}{g}\hat{\mathbf{w}}\right)+sg_r\hat{\psi}\hat{\mathbf{w}}+sg\hat{\mathbf{c}}-\frac{2sg}{r}\hat{\mathbf{d}}+sg\hat{\mathbf{f}}=sg(\hat{\psi}_r\hat{\mathbf{w}}_r-\hat{\mathbf{w}}\hat{\psi}_r),$$

$$\hat{\hat{\boldsymbol{\Psi}}}_\eta=\frac{s}{g}\hat{\hat{\mathbf{u}}}-\frac{g_\eta}{g}\hat{\hat{\boldsymbol{\Psi}}}, \qquad \hat{\mathbf{u}}_\eta=\frac{s}{g}\hat{\mathbf{w}}, \tag{21}$$

where

$$\hat{\mathbf{u}}=\begin{pmatrix}\hat{\psi}_z\\ q_z\\ \theta_z\end{pmatrix}, \qquad \hat{\mathbf{w}}=\begin{pmatrix}\hat{\psi}_{zz}\\ q_{zz}\\ \theta_z\end{pmatrix}, \qquad \hat{\mathbf{c}}=\begin{pmatrix}\hat{\psi}_{zz}\psi_z\\ q_{zz}\hat{\phi}_z-q_z^2\\ 0\end{pmatrix}, \qquad \hat{\mathbf{d}}=\begin{pmatrix}0\\ q_z\hat{\psi}_z\\ \theta\end{pmatrix},$$

$$\hat{\mathbf{f}}=\frac{1}{F}\begin{pmatrix}f_1\\ f_2\\ 0\end{pmatrix} \qquad \hat{\hat{\boldsymbol{\Psi}}}=\begin{pmatrix}\hat{\psi}\\ q\end{pmatrix}, \qquad \hat{\hat{\mathbf{u}}}=\begin{pmatrix}\hat{\psi}_z\\ q_z\end{pmatrix}, \tag{22}$$

subject to boundary conditions

$$\hat{\hat{\boldsymbol{\Psi}}}=0 \quad \text{and} \quad \hat{\mathbf{u}}=(0,0,1)^{\mathrm{T}} \quad \text{on } \eta=0,$$

$$\hat{\hat{\boldsymbol{\Psi}}}_{zz}=0, \quad \hat{\psi}_r+q=0 \quad \text{and} \quad \theta=0 \quad \text{on } \eta=1. \tag{23}$$

Equations (21) and (22) can be solved along lines AB and AC using a marching strategy. That is, the solution at location I along $0\leqslant\eta\leqslant1$ can be obtained provided J is known. Hence we can obtain the solution along these lines provided the solution at A is known. The equations at A are obtained from (21) by letting $r\to0$ and setting $q=0$ since the flow is initially axisymmetric. This makes $sg=0$, giving equations with only η-derivates. The corresponding boundary conditions are

$$\hat{\psi}=0, \quad \hat{\psi}_z=0 \quad \text{and} \quad \theta=1 \quad \text{on } \eta=0,$$

$$\hat{\psi}=\gamma \quad \text{and} \quad \theta=0 \quad \text{on } \eta=1 \quad \text{and} \quad \bar{h}=\gamma. \tag{24}$$

Two-dimensional model

Equations (10) and (11) are transformed in a similar fashion to (8) and (9). They are obtained by setting $\psi=0$ and $\partial/\partial x=0$ in equations (15). The growing boundary layer in this geometry varies as $y^{1/2}$ and the appropriate transformation replacing (16) is

$$z=\frac{y^{1/2}\eta\bar{h}}{y^{1/2}+1-\eta}, \qquad g=\frac{y^{1/2}}{y^{1/2}+1-\eta}, \tag{25}$$

with $\bar{h}=h$. Setting $\xi=y^{1/2}$, formulae (17) are the same except that the non-zero part of $s\bar{\nabla}g$ is

$$sg_y=\frac{(1-\eta)(\xi+1)\bar{h}}{2(\xi+1-\eta)^4}. \tag{26}$$

Since $\psi=0$, three equations are redundant, giving a system of five equations. The boundary conditions are the same as (24) if $\hat{\psi}$ is replaced by ϕ and γ by γ_2. For full details see Paper I.

4. NUMERICAL PROCEDURE

Solution of the boundary equations and the two-dimensional model

The boundary equations (21) are solved numerically using a modification of the Keller box method described in Paper I. Although full details are given in that paper, a brief account will be given here in order that the new features appearing in the three-dimensional model can be addressed.

A grid is placed in the two-dimensional domain $r \geqslant 0$, $0 \leqslant \eta \leqslant 1$, which is not necessarily uniform, given by the nodal points $r_i = r_{i-1} + k_i$, $i = 1, 2, \ldots$, $\eta_k = \eta_{k-1} + h_k$, $k = 1, 2, \ldots, N$, where $r_0 = 0$, $\eta_0 = 0$, $\eta_N = 1$ and N is the number of mesh spaces in the η-direction. Equations (21) are a set of eight first-order non-linear equations. The first three equations (i.e. the first vector equation) are differenced about the centre of a mesh rectangle, i.e. about the point $(r_i - \frac{1}{2}k_i, \eta_k - \frac{1}{2}h_k)$, using simple central differences and averaging to obtain a second-order scheme. Since the other five equations do not contain derivatives in r, they are more conveniently differenced about the point $(r_i, \eta_k - \frac{1}{2}h_k)$. Since these equations will be solved by a marching procedure, variables up to and including r_{i-1} (i.e. as far as location I in Figure 3) will be known and the differenced equations together with the boundary conditions (23) will form a set of $8N+9$ non-linear equations in as many unknowns (which are the variables $\hat{\bar{\Psi}}$, $\hat{\mathbf{u}}$, $\hat{\mathbf{w}}$ and $\bar{h}$ at location r_i, i.e. J in Figure 3). This set of equations is solved using Newton's method with the value of the variables at r_{i-1} as a starting value. The ensuing Jacobian is a banded matrix with the final column filled owing to $\bar{h}$ being in all the equations. Inversion of this matrix is described in Paper I.

The initial equations at location A are all differenced about $(r_0, \eta_k - \frac{1}{2}h_k)$ and the resulting system is again solved by Newton's method. Equations (25) for the two-dimensional model are solved in a similar way; in this case there are $5N+6$ equations in the system.

Solution of the three-dimensional equations

Having solved the boundary equations, we solve the three-dimensional equations (15) in the domain $x>0$, $y>0$ using a similar technique. A grid $x_i = x_{i-1} + k_i^x$, $i = 1, 2, \ldots$, $y_j = y_{j-1} + k_j^y$, $j = 1, 2, \ldots$, with $x_0 = y_0 = 0$ and η_k as before, is placed on the domain. The equations are differenced about $(x_i - \frac{1}{2}k_i^x, y_j - \frac{1}{2}k_j^y, \eta_k - \frac{1}{2}h_k)$ using simple central differences and averaging as previously. Since the solution at locations E, F and G in Figure 3 will have already been obtained via the marching strategy, the solution of the variables at H can again be obtained by solving the ensuing $8N+9$ equations using Newton's method. If f is a typical variable then a suitable starting value for Newton's iteration is

$$f_H \approx f_F + f_G - f_E. \tag{27}$$

Near the jet the x- and y-components of velocity are x/r and y/r respectively, which have singular derivatives in the x- and y-directions as $r \to 0$. In order to obtain accurate numerical results, it is necessary to subtract out this singularity. This is accomplished by replacing ψ and ϕ by $\tilde{\psi}$ and $\tilde{\phi}$ via

$$\psi = \tilde{\psi} + \frac{x}{r}\hat{\psi}_0, \qquad \phi = \tilde{\phi} + \frac{y}{r}\hat{\psi}_0, \tag{28}$$

where $\hat{\psi}_0 = \hat{\psi}(0, \eta)$. This could be done algebraically by substituting (28) into the transformed equations (15). However, this produces very complicated equations and it is much easier to make the substitution at the programming stage. Arrays are set up to hold the tilded variables and each

occurrence of ψ and ϕ in the programme is replaced by the right-hand sides of (28), where $\tilde{\psi}$ and $\tilde{\phi}$ will be suitable averaged quantities (since these values are required at non-nodal points). The four derivative terms are replaced in a similar fashion by the right-hand sides of

$$\psi_x = \tilde{\psi}_x + \frac{y^2}{r^3}\hat{\psi}_0, \qquad \phi_x = \tilde{\phi}_x - \frac{xy}{r^3}\hat{\psi}_0,$$

$$\psi_y = \tilde{\psi}_y - \frac{xy}{r^3}\hat{\psi}_0, \qquad \phi_y = \tilde{\phi}_y + \frac{x^2}{r^3}\hat{\psi}_0, \tag{29}$$

where $\tilde{\psi}_x$, $\tilde{\phi}_x$, $\tilde{\psi}_y$ and $\tilde{\phi}_y$ will be approximated by their differenced counterparts. Replacing ψ by ψ_z and ψ_{zz} and ϕ by ϕ_z and ϕ_{zz} throughout equations (28) and (29) gives the corresponding equations for the derivatives of z. The procedure works well, giving smooth and accurate results near the origin.

5. RESULTS AND DISCUSSION

With three parameters (F, γ, σ) to vary it is not possible to present full results covering the whole domain. We present full results for three cases, namely $F=2$, $\sigma=1$ for $\gamma=\frac{1}{2}$, 3 and 20, which give the flavour of what happens in general. Figure 4 shows the surface velocity magnitude contours, Figure 5 the film thickness and Figure 6 the streamlines superimposed on the contours of the heat transfer coefficient defined by

$$Q = -\left.\frac{\partial\theta}{\partial z}\right|_{z=0} = \frac{1}{T_s - T_w}\left(\frac{av}{U_0}\right)^{1/2}\left.\frac{\partial T}{\partial R}\right|_{R=a}. \tag{30}$$

Perhaps the most interesting feature of the results is that the flow halts at a finite distance in the x-direction. This can be seen most clearly from Figure 7, which depicts the surface velocity along the top generator of the cylinder (i.e. $y=0$) for the three cases. The flow stops when $u=0$ at $x=x_s$, say, which we will refer to as the 'edge', and the flow does not exist for $x>x_s$. Further, for $y>0$ the flow does not exist beyond x_s since there are no non-inertial horizontal forces present and the flow is confined to a domain $0\leqslant x\leqslant x_s$, $0\leqslant y\leqslant\pi$. As x_s is approached, the derivatives of some of the varibles become singular and for accuracy reasons it is necessary to approach the edge with decreasing grid spacings. If x_i and x_{i-1} are the last two positions at which calculations have been made with corresponding values u_i and u_{i-1} for the surface velocity at $y=0$ then

$$x_s \approx x_s^i = \frac{u_i x_{i-1} - u_{i-1} x_i}{u_i - u_{i-1}}. \tag{31}$$

Approaching x_s geometrically, the next grid position is $x_{i+1} = x_i + \lambda(x_s^i - x_i)$ with $0<\lambda<1$, where λ is set to 0·5 in the calculations. Using this technique, it is possible to approach x_s to within 10^{-4}–10^{-3}. Table I gives the position of the edge for various values of F and γ (it is independent of σ). There is no obvious formula relating x_s to F and γ but a least squares fit on the data gives

$$x_s \approx 1{\cdot}66\, F^{0{\cdot}23}\gamma^{0{\cdot}36}, \tag{32}$$

which is accurate to about 5%, showing that x_s varies slowly with both F and γ.

In order to estimate the error, two runs were made with different grid spacings for each parameter set. From the differences between the results and noting that the scheme is second-order-accurate, the errors in results on the finer of the grids could be estimated. These are shown in Table II and indicate a typical accuracy of 0·03% away from the edge and 0·2% near the edge.

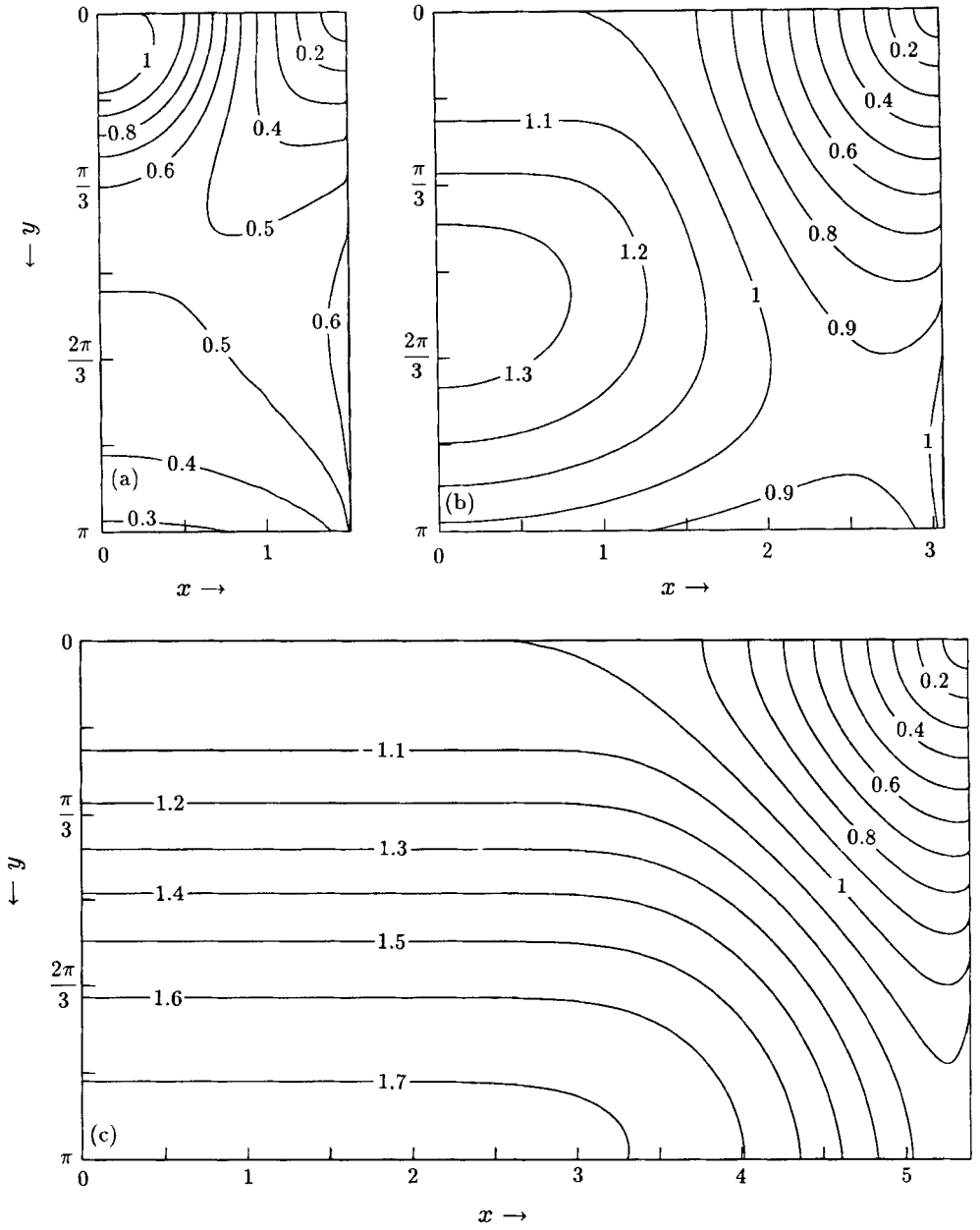

Figure 4. Surface velocity magnitude contours for $F=2$, $\sigma=1$ and (a) $\gamma=\frac{1}{2}$, (b) $\gamma=3$ and (c) $\gamma=20$

The fine grid dimensions are also shown in table, with the coarser grid being two-thirds of these in each direction. The CPU time for the fine grid runs 12, 24 and 36 h for the three values of γ on a Nimbus VX386 machine using a Fortran 386 compiler from the University of Salford.

The data in Tables I and III were derived from results on a coarse grid (the grid spacing being a factor of three larger in the x- and y-directions and $\frac{3}{2}$ in the η-direction). The CPU time was

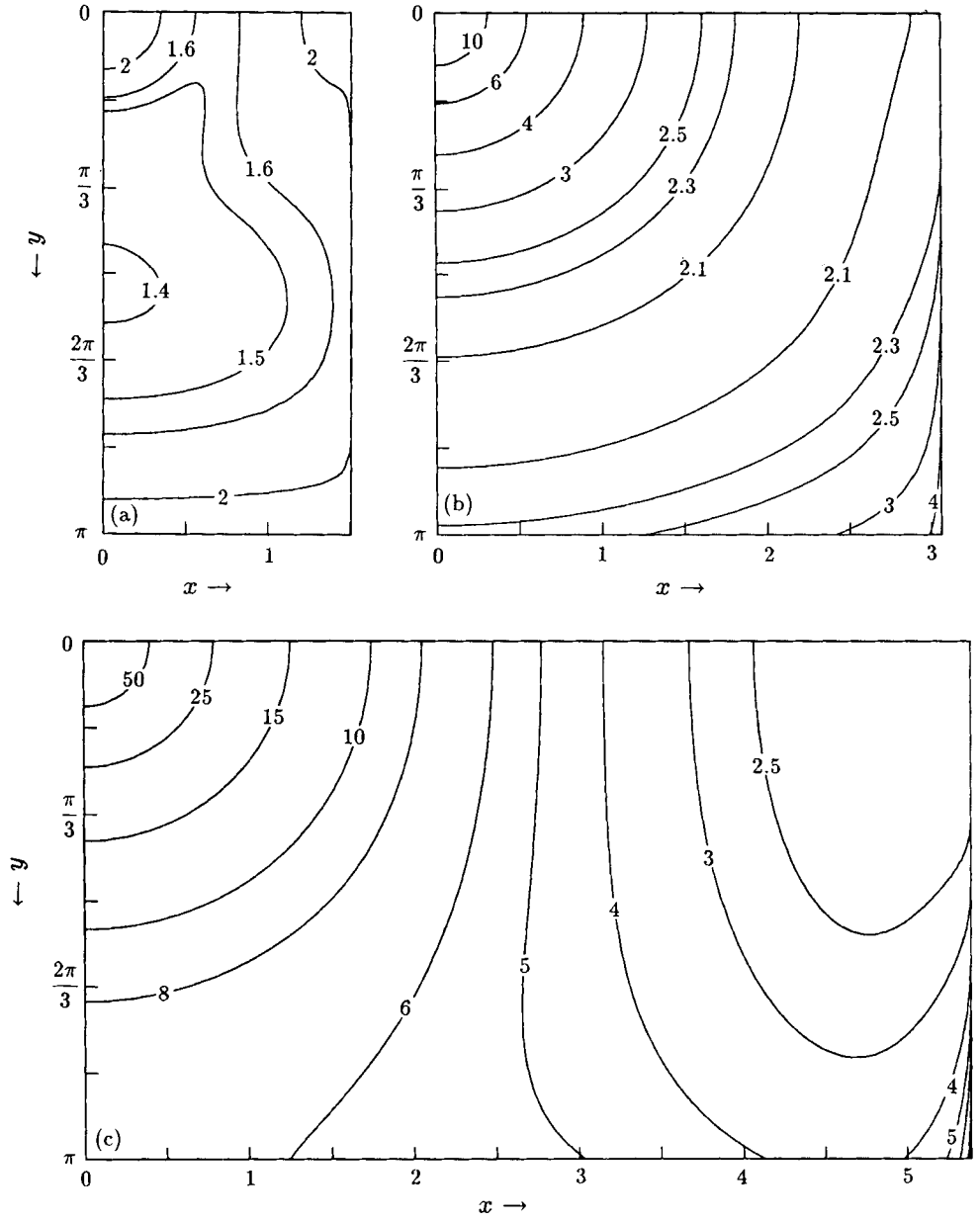

Figure 5. Film thickness contours for $F=2$, $\sigma=1$ and (a) $\gamma=\frac{1}{2}$, (b) $\gamma=3$ and (c) $\gamma=20$

typically 2 h and enabled results for a range of values of both F and γ to be obtained. Comparison with the fine grids results indicates an accuracy of about 0·3%.

Comparison with two-dimensional model

Explicit results for the two-dimensional model have been reported elsewhere (Paper I) and will therefore not be repeated here. We will compare the results of the three-dimensional model with

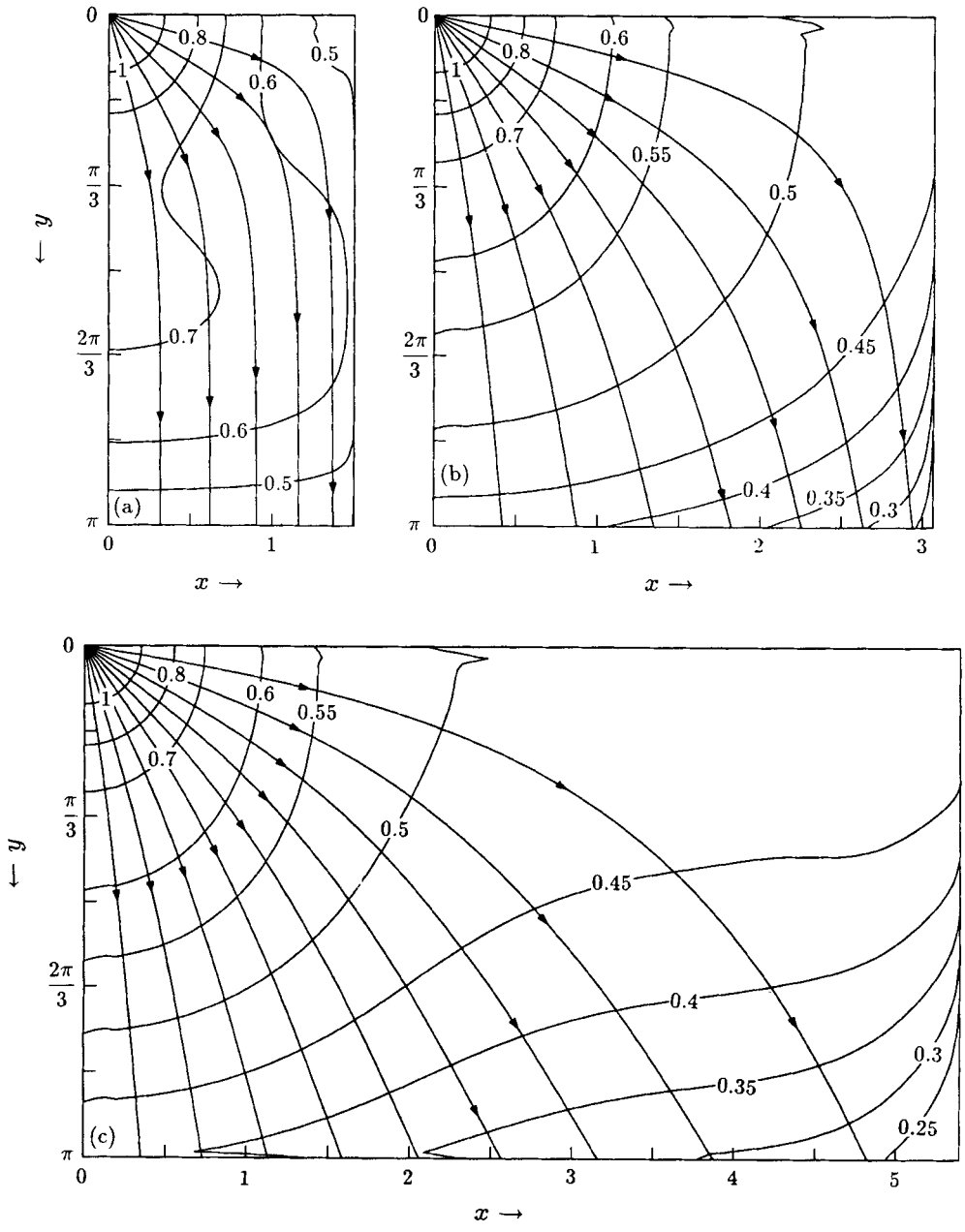

Figure 6. Heat transfer coefficient contours superimposed on streamlines for $F=2$, $\sigma=1$ and (a) $\gamma=\frac{1}{2}$, (b) $\gamma=3$ and (c) $\gamma=20$

those of the two-dimensional model which has the same initial velocity U_0, the same Froude number F and the same rate of fluid delivered per unit length of the cylinder. This last criterion gives a relationship between γ and γ_2. The cylindrical jet of the three-dimensional model creates a thin film of width $2ax_s$ (in original units), giving $\pi H_0^2 R_0/2ax_s$ as the rate per unit length. For the

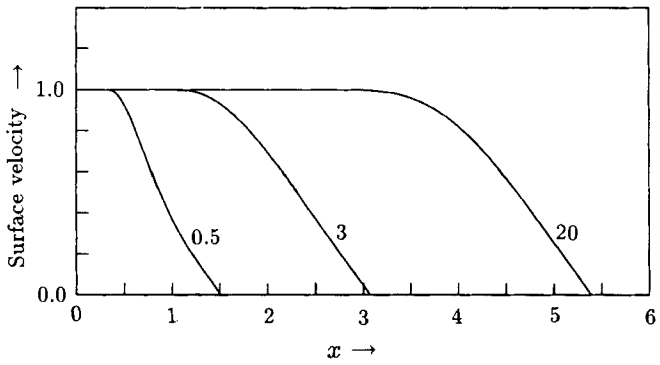

Figure 7. Surface horizontal velocity along the top generator of the cylinder for $\gamma=\frac{1}{2}$, 3 and 20

Table I. Position of the edge, x_s, as a function of F and γ

	γ					
F	0·5	1	2	5	10	20
1	1·328	1·754	2·258	3·021	3·652	4·311
2	1·503	2·020	2·650	3·643	4·490	5·394
5	1·745	2·389	3·204	4·558	5·771	7·112
10	1·935	2·680	3·645	5·307	6·855	8·621

Table II. Average relative error ($\times 10^3$) away from and near the edge for $F = 2$ and various γ

	$\gamma = 0{\cdot}5$		$\gamma = 3$		$\gamma = 20$	
	Away	Near	Away	Near	Away	Near
Horizontal velocity u	0·1	0·1	0·1	0·2	0·1	0·1
Vertical velocity v	0·3	6·9	0·1	0·6	0·1	0·2
Heat flux Q	0·3	1·7	0·2	0·4	2·0	1·4
Film thickness h	0·3	9·4	0·2	2·7	0·2	2·3
Grid dimensions	66 × 90 × 96		72 × 90 × 96		108 × 90 × 96	

two-dimensional model this rate is $2H_2U_0$. Equating the two rates and using the definitions of γ and γ_2 to eliminate H_0 and H_2 gives

$$\gamma_2=\frac{\pi\gamma}{2x_s} \tag{33}$$

as the required relationship.

Figure 8 shows contour maps of the ratio 3D/2D of the results when $F=2$ and $\gamma=\frac{1}{2}$ for vertical edge velocity, film thickness and heat transfer coefficient. For $0\leqslant y\leqslant\pi/3$ the comparison is poor, as would be expected since the differences between the two geometries are most apparent here. However, for $\pi/3\leqslant y\leqslant\pi$ the comparison is quite good, showing differences of the order of at most

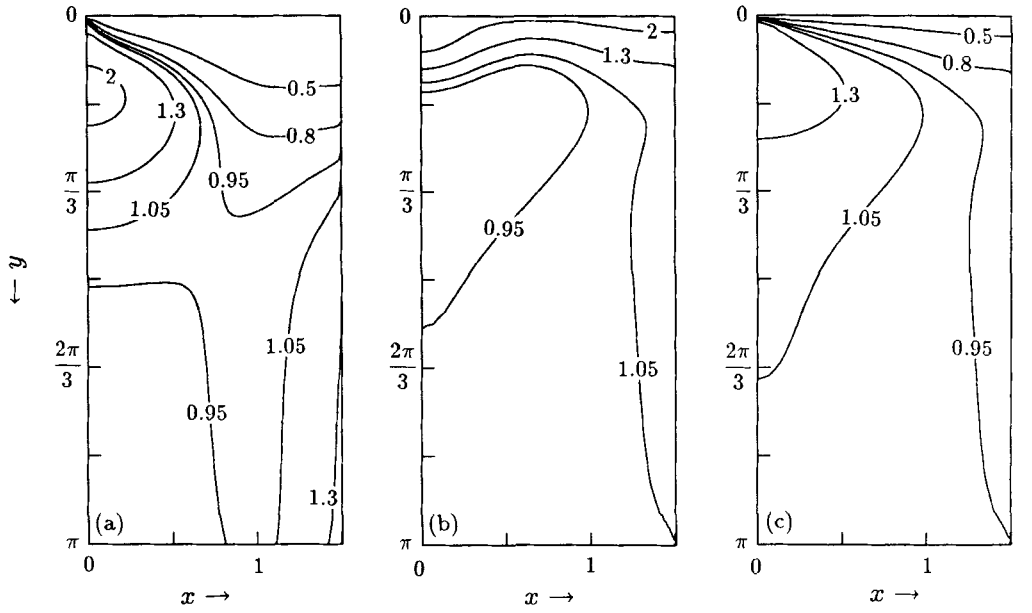

Figure 8. Contours showing the ratio of results from the two- and three-dimensional models for $F=2$, $\gamma=\frac{1}{2}$ and $\sigma=1$: (a) surface vertical velocity; (b) film thickness; (c) heat transfer coefficient

10%. We can 'average' out these differences in the x-direction using formula

$$\bar{g}(y)=\frac{1}{x_s}\int_0^{x_s} g(x, y)\,dx, \tag{34}$$

where g is a representative function. The 'averaged' ratios for surface vertical velocity, film thickness and heat transfer coefficient are shown in Figure 9 for $F=2$ with various γ. In the case $\gamma=\frac{1}{2}$ for $\pi/3\leqslant y\leqslant\pi$ the results are very close, having differences of about 1%; however, as γ increases, the comparison becomes increasingly worse. We can ascertain the effect of the region $0\leqslant y\leqslant\pi/3$ by calculating the global average, i.e. forming

$$\bar{g}=\frac{1}{\pi}\int_0^{x_s}\bar{g}(y)\,dy. \tag{35}$$

Table III lists the percentage differences in the global averages for surface vertical velocity, film thickness, heat transfer coefficient and surface velocity magnitude for various F and γ with $\sigma=1$. From the table it is clear that there is a gradual worsening of the correlation between the two models as both γ and F increase. Comparing these percentage differences with the position of x_s as shown in Table I, it is clear that the differences between the two models are related to the distance from the jet to the edge. Although the surface vertical velocity and film thickness are considerably different for the two models at large γ, the heat transfer coefficient is not so dissimilar, with an average difference of only 3%. Since our main interest is how thin films affect the heat transfer characteristics of horizontal tubes in a heat exchanger, it is apparent that the two-dimensional model will give the correct overall result to within this percentage. Hence the two-dimensional model can be used with reasonable confidence in spite of the fact that the source of liquid is

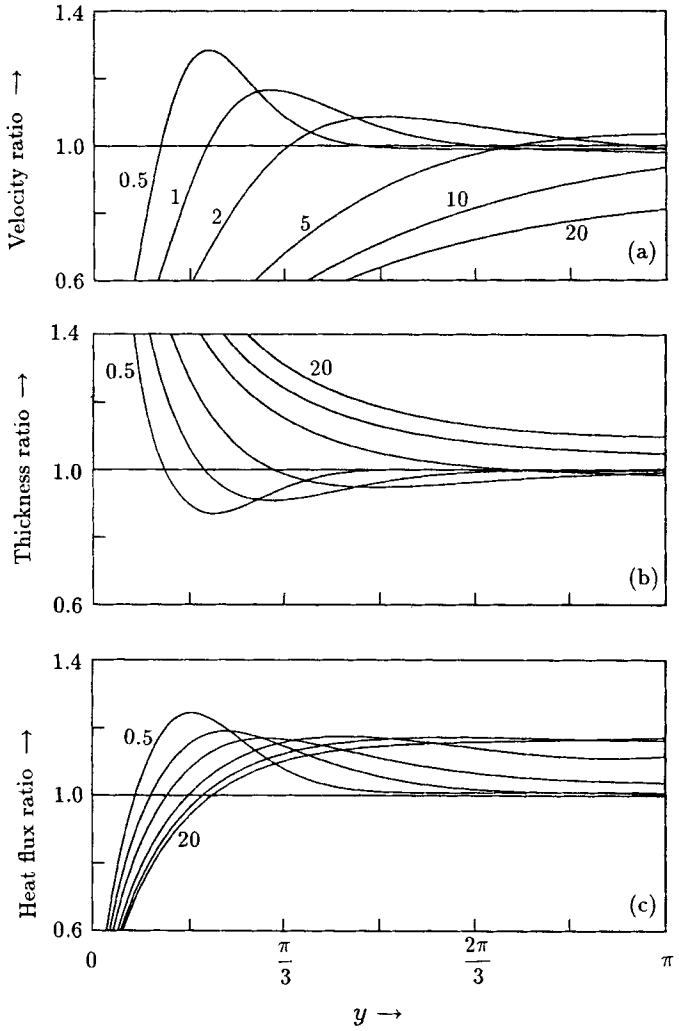

Figure 9. Ratio of results from the two- and three-dimensional models averaged in the x-direction for various values of γ: (a) surface vertical velocity; (b) film thickness; (c) heat transfer coefficient

columns rather than a sheet. Finally in the table are given the differences in surface velocity magnitude, which are much closer than the vertical velocity.

In a heat exchanger we do not have a single jet but a series of columns of liquid falling onto the tubes at more or less equally spaced intervals (Figure 1(a)). If these columns are modelled by a vertical sheet then it is intuitive that the closer the columns are together, the more accurate will be the result. The question that arises is how accurate can we except the two-dimensional model to be for a given column separation L. Assuming that a series of columns can be modelled approximately by a set of single columns whose edge (x_s) is at a distance $\frac{1}{2}L$, then we can use Table III to estimate the likely error incurred. As mentioned earlier, the error incurred is correlated to the position of the edge, and in Figure 10 we give a least squares fit to the errors incurred by the surface vertical velocity and the heat transfer coefficient as a function of edge

Table III. Percentage differences between the global averages of the two-dimensional and three-dimensional models for $\sigma = 1$

		γ					
	F	0·5	1	2	5	10	20
Surface vertical velocity	1	6·1	8·9	11·4	15·7	19·4	21·0
	2	6·8	10·5	14·1	20·6	26·3	29·4
	5	7·3	11·9	16·8	26·6	35·6	41·3
	10	7·0	12·1	17·9	30·1	41·5	49·3
Film thickness	1	4·0	7·1	11·3	18·2	23·0	26·7
	2	3·4	6·4	10·9	19·5	26·1	31·3
	5	2·4	5·1	9·5	20·8	30·9	39·0
	10	1·6	3·9	7·9	21·4	35·2	46·2
Heat transfer coefficient	1	1·5	1·7	3·2	6·0	5·5	3·4
	2	1·3	1·0	1·8	3·6	2·9	0·6
	5	1·3	0·3	0·0	0·5	2·1	5·0
	10	1·5	0·0	1·0	3·8	6·8	10·4
Surface velocity magnitude	1	1·3	0·2	1·5	3·9	6·1	6·2
	2	3·1	1·3	0·2	3·9	7·5	8·3
	5	6·8	5·1	3·4	2·3	8·6	11·3
	10	10·7	9·4	7·6	0·2	8·4	13·3

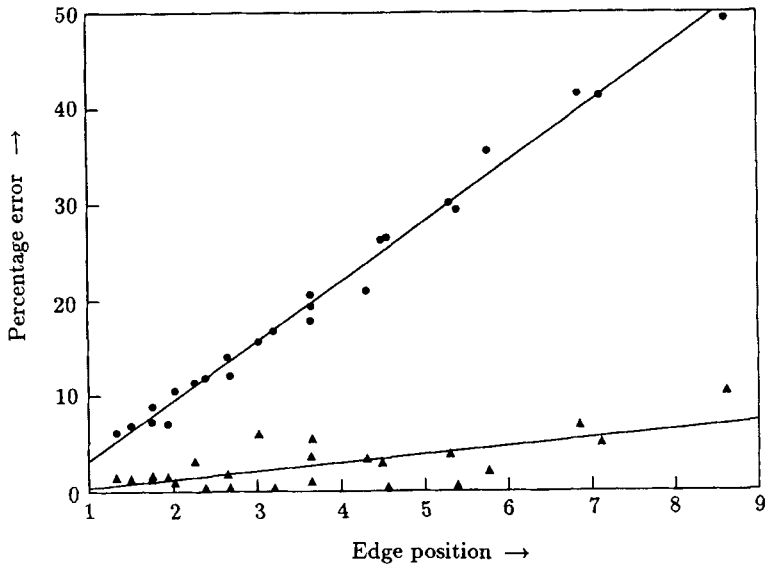

Figure 10. Least squares straight line fits to the errors incurred when the jet of liquid is replaced by a vertical sheet for the surface vertical velocity (circles) and heat transfer coefficient (triangles). The lines are $6{\cdot}26x_s - 3{\cdot}10$ and $0{\cdot}86x_s - 0{\cdot}48$ respectively. The corresponding line for the film thickness is $6{\cdot}29x_s - 6{\cdot}40$

position. From the slope of the lines we can conclude that the representation of a series of columns by a uniform sheet incurs percentage errors $6{\cdot}3\lambda$ and $0{\cdot}9\lambda$ in the velocity and heat flux fields respectively, where $\lambda = L/D$ with D being the diameter of the tubes. Since our main interest lies in the heat transfer characteristics of the tubes, it is the latter of these formulae which is the more significant. The error in the film thickness is similar to that of the velocity.

6. CONCLUSIONS

Numerical results have been obtained for the thin film flow surrounding a cylinder, issuing from a single cylindrical vertical jet. These have been obtained on fine grids for three cases ($F = 2$; $\gamma = \frac{1}{2}$, 3, 20; $\sigma = 1$) with an accuracy of about 0·07% and coarse grids for 24 cases ($F = 1$, 2, 5, 10; $\gamma = \frac{1}{2}$, 1, 2, 5, 10, 20; $\sigma = 1$) with an accuracy of about 0·3%.

The flow terminates at a finite distance in the x-direction. This distance increases slowly with F and γ.

A comparison with an equivalent two-dimensional model shows that the difference in the average heat transfer coefficient is typically about 3%.

The replacement of a series of columns by a vertical sheet incurs typical errors of 6% times the separation/diameter ratio for the velocity and film thickness and 1% for the heat flux.

REFERENCES

1. R. Hunt, 'The numerical solution of parabolic free boundary problems arising from thin film flows', *J. Comput. Phys.*, **84**, 377–402 (1989).
2. M. A. Abdelghaffar, A. A. Nicol, R. J. Gribben and G. Wilks, 'Thin film inundation flow over a horizontal cylinder', *Math. Eng. Ind.*, **2**, 143–155 (1988).
3. R. J. Gribben, R. Hunt, M. A. Abdelghaffar and G. Wilks, 'Evaluation of the approximate treatment of thin film flows', *Appl. Math. Model.*, **14**, 420–426 (1990).
4. A. A. Nicol, Z. L. Aidoun, R. J. Gribben and G. Wilks, 'Heat transfer in the presence of condensate drainage', *Int. J. Multiphase Flow*, **14**, 349–359. (1988).
5. A. A. Nicol, M. A. Abdelghaffar, G. Wilks and R. J. Gribben, 'A theory for condensation with drainage', *Second U.K. National Heat Transfer Conf.*, Mechanical Engineering Publications, London, 1988.
6. J. Crank, *Free and Moving Boundary Problems*, Oxford Press (Clarendon), London/New York, 1984.